Inorg. Chem. **2002**, *41*, 727−737

Carbamoylphosphine Oxide Complexes of Trivalent Lanthanide Cations: Role of Counterions, Ligand Binding Mode, and Protonation Investigated by Quantum Mechanical Calculations

C. Boehme and G. Wipff*

Laboratoire MSM, UMR CNRS 7551, Institut de Chimie, 4 rue B. Pascal, 67 000 Strasbourg, France

Received June 20, 2001

We present a quantum mechanical study of carbamoylphosphine oxide (CMPO) complexes of MX_3 (M^{3+} = La^{3+}, Eu^{3+}, Yb^{3+}; X^- = Cl^-, NO_3^-) with a systematic comparison of monodentate vs bidentate binding modes of CMPO. The per ligand interaction energies ΔE increase from La^{3+} to Yb^{3+} and are higher with Cl^- than with NO_3^- as counterions, as a result of steric strain in the first coordination sphere with the bidentate anions. The energy difference between monodentate (via phosphoryl oxygen) and bidentate CMPO complexes is surprisingly small, compared to ΔE or to the binding energy of one solvent molecule. Protonation of uncomplexed CMPO takes place preferably at the phosphoryl oxygen O_P, while in the $Eu(NO_3)_3CMPOH^+$ complex carbonyl (O_C) protonation is preferred and O_P is bonded to the metal. A comparison of uranyl and lanthanide nitrate complexes of CMPO shows that the interaction energies ΔE of the former are lower. Finally, the effect of grafting CMPO arms at the wide rim of a calix[4]arene platform is described. The results are important for our understanding of cation binding and extraction by potentially bidentate CMPO, diamide, and diphosphoryl types of ligands.

1. Introduction

Nuclear fuel reprocessing is based on the dissolution of irradiated material in nitric acid solution, from which it would be highly desirable to separate the different radioactive components with respect to their lifetime, for further processing and disposal.[1−3] In this context, two phosphoryl-containing ligands, TBP (tri-*n*-butyl phosphate) and CMPOs (Figure 1) are used in liquid−liquid extraction processes. In the PUREX (plutonium uranium refining by extraction) process TBP extracts uranyl and plutonyl cations to an organic phase, leaving most of the trivalent actinides such as Am^{III} and the lanthanides in the aqueous phase. The latter can be efficiently extracted by bifunctional neutral extractants such as CMPOs, as used in the American TRUEX (trans-uranium extraction) process, which is based on *N*,*N*-diisobutyl-2-(octylphenylphosphinyl)acetamide (R_1 = octyl, R_2 = phenyl; R_3 = R_4 = isobutyl; see Figure 1), while the Russian variant uses other derivatives (e.g. R_1 = R_2 = phenyl or butyl; R_3 = R_4 = ethyl).[4−10] CMPO groups may also be grafted on molecular preorganized platforms such as calixarenes[11−13] or resorcinarenes,[14−16] leading to marked extraction enhancement, compared to CMPO itself. Still,

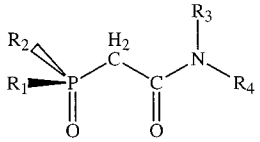

Figure 1. Schematic representation of CMPO (R_1 = R_2 = R_3 = R_4 = methyl in **L**).

* Corresponding author. E-mail: wipff@chimie.u-strasbg.fr.

(1) Choppin, G. R.; Nash, K. L. *Radiochim. Acta* **1995**, *70/71*, 225−236.
(2) Nash, K. L. *Solvent Extr. Ion Exch.* **1993**, *11*, 729−768.
(3) Cecille, L.; Casarci, M.; Pietrelli, L. *New Separation Chemistry Techniques for Radioctive Waste and other Specific Applications*; Commission of the European Communities; Elsevier Applied Science: London, New York, 1991.
(4) Horwitz, E. P.; Kalina, D. G.; Diamond, H.; Vandegrift, G. F.; Schultz, W. W. *Solvent Extr. Ion Exch.* **1985**, *3*, 75−109.
(5) Horwitz, E. P.; Diamond, H.; Martin, K. A. *Solvent Extr. Ion Exch.* **1987**, *5*, 447−470.
(6) Mathur, J. N.; Murali, M. S.; Natarajan, P. R.; Badheka, L. P.; Banerji, A. *Talanta* **1992**, *39*, 493−496.
(7) Liansheng, W.; Gasparini, G. M. *ENEA Report ISSN/0393-6252* **1990**, 1−57.
(8) Horwitz, E. P.; Martin, K. A.; Diamond, H.; Kaplan, L. *Solvent Extr. Ion Exch.* **1986**, *4*, 449−494.
(9) Chmutova, M. K.; Litvina, M. N.; Pribylova, G. A.; Nesterova, N. P.; Klimenko, V. E.; Myasoedov, B. F. *Radiochemistry* **1995**, *37*, 396−400.
(10) Litvina, M. N.; Chmutova, M. K.; Myasoedov, B. F.; Kabachnik, M. I. *Radiochemistry* **1996**, *38*, 494−499.

10.1021/ic010658t CCC: $22.00
Published on Web 01/25/2002

further separation of trivalent lanthanides from the actinides, for the purpose of vitrification, remains a challenging task.

It is generally accepted that multidentate ligands are preferred over groups of monodentate ligands,[17] but the basis of their selectivity remains poorly understood. Thus, the question of binding of CMPO is also of interest for other classes of difunctional ligands such as diphosphine oxides,[18,19] β-diketones,[20,21] diamides,[22−24] picolinamides,[23,25] podands,[26] or polypyridines,[27−29] which also bind lanthanide or actinide cations. Solid-state structures confirm that CMPO derivatives or analogues with phosphine oxide, phosphinate, or phosphonate groups bind to the lanthanide or uranyl cations generally in a bidentate mode, but monodentate binding by the phosphoryl O_P oxygen is also observed.[30−33] In solution, the Am^{3+} complex is believed to involve three CMPO molecules, whose phosphoryl and carbonyl functions participate in the complexation, three NO_3^- anions, and three coextracted HNO_3 molecules.[34] There has been so far, to our knowledge, no direct comparison of the monodentate vs bidentate binding mode. Following a systematic investigation on simple ligands binding to lanthanide ions,[35−44] we decided to investigate by quantum mechanical (QM) methods several aspects of M^{3+} lanthanide binding to CMPO: the ligand binding mode; the relation between proton vs metal basicity of the ligand; the effect of counterions and of the cation hardness on CMPO coordination; the effect of CMPO attachment to a molecular platform; the comparison of M^{3+} lanthanide with uranyl binding to CMPO.

In contrast to force field approaches, which assume a fixed electronic representation of the system (for general papers see e.g. refs 45−49, and for earlier modeling studies on CMPO see refs 50−53), QM accounts for structural and electronic reorganization effects as a function of the conformation of the ligands and coordination and environment of the metal. The main problems in the QM treatment of lanthanides and actinides are relativistic effects and the near degeneracy of the f orbitals. For the lanthanides these problems can be avoided by replacing the explicit treatment of the core orbitals by an implicit one, i.e., by using relativistic effective core potentials (ECP). The latter include the highly stabilized f orbitals, which usually do not contribute to chemical properties.[54−57] Because the inclusion of f orbitals into the core is not accurate enough for the actinides, many studies in this area concentrate on cations such as uranyl, where they are basically unoccupied. Applications in lanthanide or actinide coordination can be found in refs 58−62 for uranyl cations and in refs 63−67 for other cations.

In this study, we consider the tetramethyl derivative of CMPO, hereafter noted **L** (Figure 1), interacting with the

(11) Arnaud-Neu, F.; Böhmer, V.; Dozol, J.-F.; Grüttner, C.; Jakobi, R. A.; Kraft, D.; Mauprivez, O.; Rouquette, H.; Schwing-Weil, M.-J.; Simon, N.; Vogt, W. *J. Chem. Soc., Perkin Trans. 2* **1996**, 1175−1182.
(12) Delmau, L. H.; Simon, N.; Schwing-Weill, M.-J.; Arnaud-Neu, F.; Dozol, J.-F.; Eymard, S.; Tournois, B.; Böhmer, V.; Grüttner, C.; Musigmann, C.; Tunayar, A. *J. Chem. Soc., Chem. Commun.* **1998**, 1627−1628.
(13) Böhmer, V. In *Calixarenes for Separation*; ACS Symposium Series 757; Lumetta, G., Rogers, R., Gopolan, A., Eds.; American Chemical Society: Washington, DC, 2000; pp 135−148.
(14) Boerrigter, H.; Verboom, W.; Reinhoudt, D. N. *J. Org. Chem.* **1997**, *62*, 7148−7155.
(15) Boerrigter, H.; Verboom, W.; Reinhoudt, D. N. *Liebigs Ann./Recueil* **1997**, 2247−2254.
(16) Boerrigter, H.; Thomasberger, T.; Verboom, W.; Reinhoudt, D. N. *Eur. J. Org. Chem.* **1999**, *665*, 5−674.
(17) Hay, B. P.; Dixon, D. A.; Vargas, R.; Garza, J.; Raymond, K. *Inorg. Chem.* **2001**, *40*, 3922−3935.
(18) Rozen, A. M.; Nikolotova, Z. I.; Kartasheva, N. A. *Radiokhimiya* **1986**, *28*, 407.
(19) Rozen, A. M.; Krupnov, B. V. *Russ. Chem. Rev.* **1996**, *65*, 973−1000 and references therein.
(20) Wu, H.; Lin, Y.; Smart, N. G.; Wai, C. M. *Anal. Chem.* **1996**, *68*, 4072−4075.
(21) Felinto, M. C. F. C.; Almeida, V. F. *J. Alloys Compd.* **2000**, *303−304*, 524−528.
(22) Siddell, T. H., III. *J. Inorg. Nucl. Chem.* **1963**, *29*, 883−892.
(23) Nigond, L.; Condamines, N.; Cordier, P. Y.; Livet, J.; Madic, C.; Cuillerdier, C.; Musikas, C. *Sep. Sci. Technol.* **1995**, *30*, 2075−2099.
(24) Spjuth, L.; Liljenzin, J. O.; Hudson, M. J.; Drew, M. G. B.; Iveson, P. B.; Madic, C. *Solvent Extr. Ion Exch.* **2000**, *18*, 1−23.
(25) Grenthe, I. *J. Am. Chem. Soc.* **1961**, *83*, 360−364.
(26) Nazarenko, V.; Baulin, V. E.; Lamb, J. D.; Volkova, T.; Varnek, A.; Wipff, G. *Solvent Extr. Ion Exch.* **1999**, *17*, 495−523.
(27) Constable, E. C. *Adv. Inorg. Chem. Radiochem.* **1986**, *30*, 69−121.
(28) Piguet, C.; Bünzli, J.-C. G.; Bernardinelli, G.; Hopfgartner, G.; Petoud, S.; Schaad, O. *J. Am. Chem. Soc.* **1996**, *118*, 6681−6697.
(29) Kolarik, Z.; Müllich, U.; Gassner, F. *Solvent Extr. Ion Exch.* **1999**, *17*, 23−32.
(30) Bowen, S. M.; Duesler, N.; Paine, R. T. *Inorg. Chim. Acta* **1982**, *61*, 155−166.
(31) Caudle, L. J.; Duesler, E. N.; Paine, R. T. *Inorg. Chem.* **1985**, *24*, 4441−4444.
(32) Bowen, S. M.; Duesler, E. N.; Paine, R. T. *Inorg. Chim. Acta* **1982**, *59*, 53−63.
(33) Bowen, S. M.; Duesler, E. N.; Paine, R. T. *Inorg. Chem.* **1983**, *22*, 286−290.
(34) Chamberlain, D. B.; Leonard, R. A.; Hoh, J. C.; Gay, E. C.; Kalina, D. G.; Vandegrift, D. G. *Truex Hot Demonstration: Final Report ANL-89/37*; Argonne National Laboratory: Argonne, IL, Apr 1990.
(35) Hutschka, F.; Troxler, L.; Dedieu, A.; Wipff, G. *J. Phys. Chem. A* **1998**, *102*, 3773−3781.
(36) Troxler, L.; Dedieu, A.; Hutschka, F.; Wipff, G. *J. Mol. Struct. (THEOCHEM)* **1998**, *431*, 151−163.
(37) Berny, F.; Muzet, N.; Troxler, L.; Dedieu, A.; Wipff, G. *Inorg. Chem.* **1999**, *38*, 1244−1252.
(38) Schurhammer, R.; Erhart, V.; Troxler, L.; Wipff, G. *J. Chem. Soc., Perkin Trans.2* **1999**, 2515−2534.
(39) Baaden, M.; Berny, F.; Boehme, C.; Muzet, N.; Schurhammer, R.; Wipff, G. *J. Alloys Compd.* **2000**, *303−304*, 104−111.
(40) Boehme, C.; Wipff, G. *J. Phys. Chem. A* **1999**, *103*, 6023−6029.
(41) Boehme, C.; Wipff, G. *Inorg. Chem.* **1999**, *38*, 5734−5741.
(42) Boehme, C.; Wipff, G. *Chem. Eur. J.* **2001**, *7*, 1398−1407.
(43) Baaden, M.; Burgard, M.; Boehme, C.; Wipff, G. *Phys. Chem. Chem. Phys.* **2001**, *3*, 1317−1325.
(44) Berny, F.; Wipff, G. *J. Chem. Soc., Perkin Trans.2* **2001**, 73−82.
(45) Wipff, G. *J. Coord. Chem.* **1992**, *27*, 7−37.
(46) Hay, B. P. *Coord. Chem. Rev.* **1993**, *126*, 177−236 and references therein.
(47) Boeyens, J. C. A.; Comba, P. *Coord. Chem. Rev.* **2001**, *212*, 3−10.
(48) Hancock, R. D. *Acc. Chem. Res.* **1990**, *23*, 253−257.
(49) Beech, J.; Drew, M. G. B.; Leeson, P. B. *Struct. Chem.* **1996**, *7*, 153−165.
(50) Rogers, R. D.; Rollins, A. N.; Gatrone, R. C.; Horwitz, E. P. *J. Chem. Crystallogr.* **1995**, *25*, 43−49.
(51) Gatrone, R. C.; Horwitz, E. P. *Solvent Extr. Ion Exch.* **1988**, *6*, 937−972.
(52) Guilbaud, P.; Wipff, G. *New J. Chem.* **1996**, *20*, 631−642.
(53) Troxler, L.; Baaden, M.; Wipff, G.; Böhmer, V. *Supramol. Chem.* **2000**, *12*, 27−51.
(54) Maron, L.; Eisenstein, O. *J. Phys. Chem. A* **2000**, *104*, 7140−7143.
(55) Hong, G.; Schautz, F.; Dolg, M. *J. Am. Chem. Soc.* **1999**, *121*, 1, 1502−1512.
(56) Dolg, M.; Stoll, H.; Savin, A.; Preuss, H. *Theor. Chim. Acta* **1993**, *85*, 441.
(57) Dolg, M.; Stoll, H. In *Handbook on the Physics and Chemistry of the Rare Earths*; Elsevier: Amsterdam, 1996; Chapter 152, pp 607−729.
(58) Craw, J. S.; Vincent, M. A.; Hillier, I. H.; Wallwork, A. L. *J. Phys. Chem.* **1995**, *99*, 10181−10185.

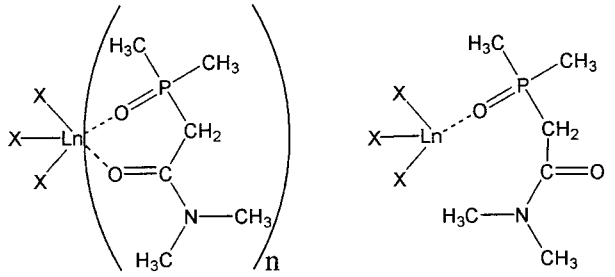

Figure 2. Schematic representation of the bidentate $MX_3\mathbf{L}$ and $MX_3\mathbf{L}_2$ complexes (n = 1 and 2, respectively) and of the monodentate $MX_3\mathbf{L}$ complex (O_P coordination).

La^{3+}, Eu^{3+}, and Yb^{3+}, lanthanide cations of decreasing size (their ionic radius is 1.032, 0.947, and 0.868 Å, respectively[68]). In terms of the HSAB approach where ligands are bases and the metals are acids,[69] the studied lanthanides are of increasing hardness, and their comparison may be also of interest in the context of actinide/lanthanide (e.g. Am^{III} vs Eu^{III}) separation, as the latter are generally considered to be somewhat harder.[70−72] We first describe neutral 1:1 $MX_3\mathbf{L}$ complexes, with $X^- = Cl^-$ vs NO_3^-. Chloride anions are used for convenience as in earlier studies,[36−43] while nitrates are of relevance in the context of nuclear waste acidic solutions. Nitrates generally bind in a bidentate mode,[73] leading to larger coordination numbers and enhanced steric repulsions in the first coordination shell, compared to monodentate anions. It is thus of interest to compare complexes with both types of anions. For selected 1:1 complexes, we compare the bidentate vs monodentate binding of CMPO to the metal, schematically shown in Figure 2. As the phosphoryl groups form stronger bonds to the metal than the amides,[37,39] monodentate binding is achieved by the O_P oxygen atom. Another matter of interest concerns the actinide complexes of CMPO, and as a first approach, we decided to also model the uranyl nitrate complex of CMPO.

Scheme 1. Definition of the Calculated Interaction Energies ΔE

$$LnX_3 + \mathbf{L} \xrightarrow{\Delta E} LnX_3\mathbf{L}$$

$$LnX_3\mathbf{L} + \mathbf{L} \xrightarrow{\Delta E} LnX_3\mathbf{L}_2$$

$$LnX_3 + \mathbf{L}H^+ \xrightarrow{\Delta E} LnX_3\mathbf{L}H^+$$

$$UO_2X_2 + \mathbf{L} \xrightarrow{\Delta E} UO_2X_2\mathbf{L}$$

In the 1:1 complexes of the $MCl_3\mathbf{L}$ type, the coordination number CN of the metal (CN = 5) is lower than the usual CN of lanthanides (from 11 to 7 depending on the lanthanide cation and the ligands). In chloroform solution, up to three CMPOs may bind to lanthanide nitrates.[74] This is why we also consider 1:2 $Eu(NO_3)_3\mathbf{L}_2$ complexes (CN = 10; see Figure 2) which better model complexation in condensed phases (solutions or solids). One important question is whether CMPO ligands remain bidentate or move to monodentate coordination when the CN is increased. The results of full optimization of complexes taken from solid-state structures are also discussed.

In highly acidic conditions, metal extraction by CMPO has to compete with protonation of the ligand. It has been suggested that CMPO behaves as monodentate ligand where the amide function acts an internal buffer for protons and protects the $M-O_P$ bond from attack from protons.[24,75] We thus decided to first model the protonated CMPO $\mathbf{L}H^+$ to compare the phosphoryl O_P vs carbonyl O_C protonation sites and to seek for possible correlations between metal and proton coordination patterns. Then, in the $Eu(NO_3)_3\mathbf{L}H^+$ 1:1 species, we investigate to which extent the metal−ligand binding strength is weakened upon protonation and compare the protonation of the ligand vs the anion.

Finally, in relation with the recently developed CMPO calixarenes,[11,12,76] we consider a model calix[4]arene ligand substituted by four CMPO arms at the wide rim, to investigate the structure of its M^{3+} complex and the CMPO binding mode under topological constraints imposed by the calixarene platform: Are the four CMPOs equally involved in the cation coordination? How do the phosphoryl vs amidic oxygens compete to bind M^{3+}? Do different cations bind in a similar fashion? What is the effect of external counterions?

2. Methods

All compounds where fully optimized at the Hartree−Fock level of theory. The compounds **L**, MX_3, and $MX_3\mathbf{L}$ were verified as true minima on the potential hypersurface by the analytical calculation of their force constants. Binding energies ΔE have been calculated as defined in Scheme 1. In some cases the influence of electron correlation on structures and relative energies has been tested by density functional theory (DFT) calculations using the B3LYP hybrid functional. While the changes in binding energies ΔE were significant (>5 kcal/mol), the trends for the different metals and binding modes remained the same and the geometrical changes were small. In further test calculations the influence of

(59) Spencer, S.; Gagliardi, K.; Handy, N. C.; Ioannou, A. G.; Skylaris, C.-K.; Willetts, A.; Simper, A. M. *J. Phys. Chem. A* **1999**, *103*, 1831−1837.
(60) Tsushima, S.; Suzuki, A. *J. Mol. Struct. (THEOCHEM)* **2000**, 21−25.
(61) Hay, P. J.; Martin, R. L.; Schreckenbach, G. *J. Phys. Chem. A* **2000**, *104*, 6259−6270.
(62) Gagliardi, K.; Grenthe, I.; Roos, B. *Inorg. Chem.* **2001**, *40*, 2976−2978.
(63) Schreckenbach, G.; Hay, P. J.; Martin, R. L. *J. Comput. Chem.* **1999**, *20*, 70−90.
(64) Pepper, M.; Bursten, B. E. *Chem. Rev.* **1991**, *91*, 9−741.
(65) Cosentino, U.; Moro, G.; Pitea, D.; Villa, A.; Fantucci, P. C.; Maiocchi, A.; Uggerin, F. *J. Phys. Chem. A* **1998**, *102*, 4606−4614.
(66) Pyykkö, P.; Li, J.; Runeberg, N. *J. Phys. Chem.* **1994**, *98*, 4809.
(67) Vallet, V.; Maron, L.; Schimmelfpennig, B.; Leininger, T.; Teichteil, C.; Gropen, O.; Grenthe, I.; Wahlgren, U. *J. Phys. Chem. A* **1999**, *103*, 9285−9289.
(68) Katz, J. J.; Seaborg, G. T.; Morss, L. R. *The Chemistry of the Actinide Elements*, 2nd ed.; Chapman and Hall: London, 1986.
(69) Pearson, R. G. *Hard and Soft Acids and Bases*; Dowdon, Hutchinson, and Ross: Stroudsburg, PA, 1973.
(70) Choppin, G. R. In *Principles of Solvent Extraction*; Rydberg, J., Musikas, C., Choppin, G. R., Eds.; M. Dekker: New York, 1992; pp 71−100.
(71) Seaborg, G. T. *Radiochim. Acta* **1993**, *61*, 115−122.
(72) Edelstein, N. M. *J. Alloys Compd.* **1995**, *223*, 197−203.
(73) Casellato, U.; Vigato, P. A.; Vidali, M. *Coord. Chem.* **1981**, *36*, 183−265.
(74) Nakamura, T.; Miyake, C. *Solv. Extract. Ion Exch.* **1994**, *12*, 931−949.
(75) Kalina, D. G.; Horwitz, E. P.; Kaplan, L.; Muscatello, A. C. *Sep. Sci. Technol.* **1981**, *16*, 1127.
(76) Matthews, S. E.; Saadioui, M.; Böhmer, V.; Barboso, S.; Arnaud-Neu, F.; Schwing-Weill, M.-J.; Carrera, A. G.; Dozol, J.-F. *J. Prakt. Chem.* **1999**, *241*, 264−273.

Table 1. HF Results for the Studied Compounds with Distances A−B in Å, Dihedrals A−B−C−D in deg, and Metal−Ligand Binding Energies ΔE in kcal mol^{-1}

	coord[a]	M−O(P)[b]	M−O (C)[b]	O−P	O−C	M−X_I[b,c]		M−X_{II}[b,c]		M−X_{III}[b,c]		O−P− C−C	P−C− C−O	ΔE[d]
L				1.476	1.207							−70.3	−87.8	
L′				1.477	1.206							−76.3	−101.8	
$LaCl_3$**L**	bi	2.452	2.652	1.504	1.229	2.791		2.735		2.726		−53.2	7.6	−59. 0
$LaCl_3$**L**	mono	2.360	4.773	1.520	1.208	2.750		2.712		2.710		−57.1	−34.5	−51. 7
$EuCl_3$**L**	bi	2.344	2.543	1.505	1.230	2.684		2.632		2.621		−52.4	7.6	−61. 2
$EuCl_3$**L**	mono	2.253	4.812	1.521	1.208	2.641		2.608		2.605		−57.9	−38.0	−54. 8
$YbCl_3$**L**	bi	2.245	2.452	1.505	1.23 0	2.589		2.540		2.527		−51.8	7.5	−62. 2
$YbCl_3$**L**	mono	2.157	4.837	1.521	1.208	2.543		2.513		2.509		−58.7	−41.0	−57. 4
$La(NO_3)_3$**L**	bi	2.471	2.644	1.501	1.229	2.638	2.579	2.555	2.561	2.546	2.555	−55.5	4.4	−51. 5
$La(NO_3)_3$**L**	mono	2.379	4.476	1.513	1.209	2.603	2.549	2.530	2.556	2.517	2.558	−63.5	−9.7	−42. 8
$Eu(NO_3)_3$**L**	bi	2.367	2.531	1.501	1.230	2.538	2.466	2.453	2.458	2.444	2.448	−54.2	3.9	−52. 3
$Eu(NO_3)_3$ **L′**	bi	2.371	2.500	1.501	1.230	2.524	2.493	2.460	2.451	2.454	2.445	−52.5	10.4	−52. 9
$Eu(NO_3)_3$**L**	mono	2.277	4.486	1.515	1.208	2.495	2.437	2.451	2.417	2.451	2.421	−63.5	−9.7	−44. 5
$Eu(NO_3)_3$(**L**)$_2$	bi	2.431	2.560	1.490	1.217	2.560	2.673	2.673	2.530	2.519	2.529	29.7	−66.5	−21. 3
		2.474	2.589	1.494	1.224							−53.9	0.6	
$Yb(NO_3)_3$**L**	bi	2.265	2.432	1.503	1.231	2.444	2.385	2.391	2.336	2.358	2.351	−53.2	3.0	−51. 6
$Yb(NO_3)_3$**L**	mono	2.185	4.523	1.516	1.207	2.397	2.331	2.356	2.327	2.359	2.322	−65.4	−11.3	−45. 7
LH$^+$	POH^+	0.962	2.059	1.572	1.219							−54.5	4.5	
LH$^+$	COH^+	1.597	0.993	1.488	1.277							28.9	−23.9	
$Eu(NO_3)_3$**L**H$^+$	Bi, POH^+	2.747	2.486	1.588	1.237	2.471	2.433	2.401	2.428	2.428	2.412	−59.5	9.9	−12. 7
$Eu(NO_3)_3$**L**H$^+$	mono, COH^+	2.326	4.275	1.507	1.301	2.446	2.413	2.557	2.428	2.391	2.405	−26.4	−53.8	−18. 3
$Eu(NO_3)_3$**L**H$^+$	bi, NOH^+	2.324	2.383	1.514	1.242	2.442	2.406	2.405	2.414	3.240	2.620	−53.3	40.9	
[Eu(**Calix**)]$^{3+}$		2.475	2.490	1.506	1.222							38.8	−52.6	
[Yb(**Calix**)]$^{3+}$		2.391	2.416	1.507	1.222							36.8	−50.7	
Calix[e]				1.576	1.229							62.8	−3.1	
				1.580	1.229							53.8	21.9	
[Eu(**Calix**)]$^{3+}$[e]		2.458	2.416	1.511	1.246							37.8	−50.7	
[$EuCl_2$(**Calix**)]$^+$[e]		2.457	2.413	1.511	1.241							−1.2	−25.2	
		2.469	2.411	1.506	1.243							39.5	−48.3	

[a] Bidentate (Bi) or monodentate (mono) binding mode of **L**. In the case of the protonated species oxygen atom to which the proton is attached: phosphorus oxygen (POH^+), amide oxygen (COH^+), or nitrate oxygen (NOH^+). [b] M = H (in the case of the **L**H$^+$), La, Eu, and Yb, respectively. [c] X = Cl (chloride complexes) and O (nitrate complexes), respectively. [d] See Scheme 1 for definitions. [e]Calculated with the small basis set (see Methods).

the basis set superposition error (BSSE) on the relative energies ΔE turned out to be small and remained constant with different compound types, so only the uncorrected values are reported here.

The 46 core and 4f^n electrons of the lanthanides were described by a quasirelativistic effective core potential (ECP) of the Stuttgart group.[56] For the valence orbitals the affiliated (7s6p5d)/[5s4p3d] basis set was used, enhanced by an additional single f function with an exponent optimized by Frenking et al.[77] For uranium a quasirelativistic large core ECP of the Los Alamos group with 78 electrons in the core and a [3s,3p,2d,2f] contracted valence basis set was used.[78] The other atoms H, C, N, O, P, and Cl were described by the standard 6-31G(d) basis set.[79] The **Calix** complexes were at first optimized with the smaller 3-21G(d) basis set on these atoms and without f function on the lanthanides, before continuing the optimization with the larger basis set. The free **Calix** and the complex [M**Calix**Cl_2]$^+$ were only optimized with the smaller basis. In the B3LYP calculations a 6-311G(2df,p) basis set was used on the non-lanthanide atoms.

All calculations have been carried out with the Gaussian98 software.[79]

3. Results

3.1. MCl_3L Complexes: Role of the Metal Cation Hardness and the CMPO Binding Modes. In this paragraph we will discuss structures, Mulliken-derived charges, and binding energies ΔE of bidentate and monodentate CMPO (**L**) complexes of MCl_3. These complexes have a low coordination number (4−5, depending on the binding mode of **L**) and therefore allow us to investigate the structural and energy features of the metal−ligand bond without the effects of a completely filled first coordination sphere. Of course, the electronic influence of the counterions, especially on the charge of the metal cations, is also important.

Selected structural data for **L** and the MCl_3**L** complexes and the M−**L** binding energies can be found in Table 1. The structure of **L** is also shown in Figure 4; the structure of $EuCl_3$**L** with both monodentate and bidentate binding is shown in Figure 5. If one looks at the bidentate complex, it becomes clear that the M−**L** binding is not planar and the ligand is tilted from the plane formed by the metal and the oxygen binding sites. As one expects from the existence of an sp^3 phosphorus atom, carbonyl and phosphoryl bonds are not coplanar either, but the C−N−C−O(amide) part is close to planar in both the free and the complexed state. In the bidentate complexes this part is nearly rotated into one plane

(77) Ehlers, A. W.; Böhme, M.; Dapprich, S.; Gobbi, A.; Höllwarth, A.; Jonas, V.; Köhler, K. F.; Stegmann, R.; Veldkamp, A.; Frenking, G. *Chem. Phys. Lett.* **1993**, *208*, 111.

(78) Ortiz, J. V.; Hay, P. J.; Martin, R. L. *J. Am. Chem. Soc.* **1992**, *114*, 4, 2736−2737 and references therein.

(79) Frisch, M. J.; Trucks, G. W.; Schlegel, H. B.; Scuseria, G. E.; Robb, M. A.; Cheeseman, J. R.; Zakrzewski, V. G.; Montgomery, J. A., Jr.; Stratmann, R. E.; Burant, J. C.; Dapprich, S.; Millam, J. M.; Daniels, A. D.; Kudin, K. N.; Strain, M. C.; Farkas, O.; Tomasi, J.; Barone, V.; Cossi, M.; Cammi, R.; Mennucci, B.; Pomelli, C.; Adamo, C.; Clifford, S.; Ochterski, J.; Petersson, G. A.; Ayala, P. Y.; Cui, Q.; Morokuma, K.; Malick, D. K.; Rabuck, A. D.; Raghavachari, K.; Foresman, J. B.; Cioslowski, J.; Ortiz, J. V.; Stefanov, B. B.; Liu, G.; Liashenko, A.; Piskorz, P.; Komaromi, I.; Gomperts, R.; Martin, R. L.; Fox, D. J.; Keith, T.; Al-Laham, M. A.; Peng, C. Y.; Nanayakkara, A.; Gonzalez, C.; Challacombe, M.; Gill, P. M. W.; Johnson, B.; Chen, W.; Wong, M. W.; Andres, J. L.; Gonzalez, C.; Head-Gordon, M.; Replogle, E. S.; Pople, J. A. *Gaussian 98, Revision A.5*; Gaussian, Inc.: Pittsburgh, PA, 1998.

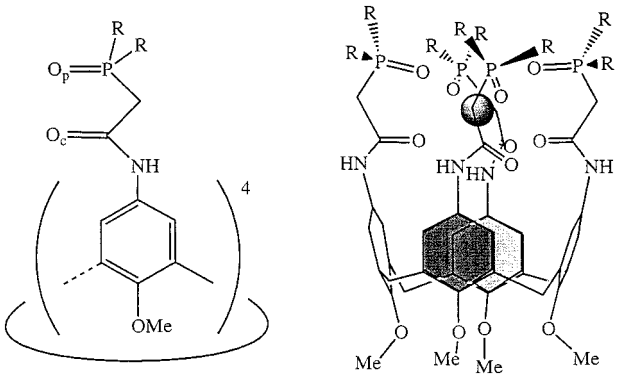

Figure 3. Schematic representation of the calculated calix[4]−CMPO ligand "**Calix**" (R = Me) and of a M^{3+} inclusion complex.

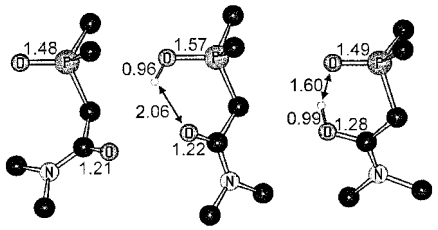

Figure 4. Structures of the free ligand **L** and the two protonated forms of $\mathbf{L}H^+$ (protonated at O_P and O_C, respectively).

with the P atom, as can be seen from the PC−CO dihedrals, which get close to 0. In the minimum energy form of the free ligand the phosphoryl and carbonyl bonds are almost in a trans position, while they are approximately perpendicular to each other in the monodentate complexes.

The M−**L** distances vary as expected with the size of the complexed metal and get smaller from La^{3+} to Yb^{3+}. In the bidentate complexes the M−O_P distance is always approximately 0.2 Å shorter than the M−O_C distance. This is an indication that the former bond is stronger than the latter, in line with the higher protonation energy of the O_P atom (vide infra). The monodentate complexes are bound via the O_P atom, and the corresponding M−O_P distance is in all cases 0.1 Å shorter than in the bidentate complexes, hinting at an increase in bond strength due to the lack of competition from the amide oxygen atom.

The bond distances within the ligand vary only slightly from the free to the complexed state and even less between the two binding modes. The different metals have almost no influence on the internal ligand structure. However, the observed bond length variations agree with expectations and the trends determined from the metal−ligand bonds. For example the P−O and C−O bonds get longer upon complexation, due to the weakening caused by the competition of the metal. From the bidentate to the monodentate binding mode the C−O bond shortens to the value found in the free ligand, while the P−O bond is weakened further and lengthens accordingly, confirming the increased M···O_P interaction also found in the shortening of the corresponding M−O bond.

Looking at the Mulliken charges (Table 2), one can see that a strengthening of an M−O bond corresponds to an increased negative charge (or, more correctly, Mulliken population) on the oxygen atom and therefore an increased

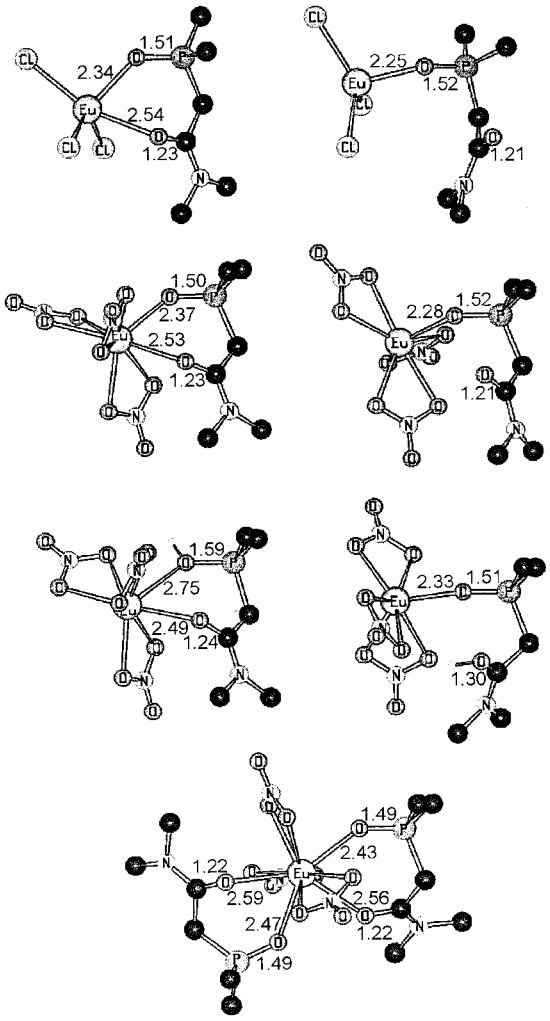

Figure 5. Structures of the calculated Europium complexes. From top to bottom: $EuCl_3\mathbf{L}$; $Eu(NO_3)_3\mathbf{L}$; protonated $Eu(NO_3)_3\mathbf{L}H^+$ bidentate (left) and monodentate (right); $Eu(NO_3)_3\mathbf{L}_2$.

Table 2. HF-Derived Mulliken Charges *Q* of **L** and Selected Complexes

		Q(M)	*Q*(O_P)	*Q*(P)	*Q*(O_C)	*Q*(C)
L			−0.74	1.28	−0.65	0.77
$LaCl_3\mathbf{L}$	bi	1.69	−0.91	1.52	−0.73	0.88
$LaCl_3\mathbf{L}$	mono	1.71	−0.97	1.51	−0.64	0.83
$EuCl_3\mathbf{L}$	bi	1.54	−0.92	1.53	−0.73	0.89
$EuCl_3\mathbf{L}$	mono	1.56	−0.97	1.51	−0.64	0.83
$YbCl_3\mathbf{L}$	bi	1.44	−0.92	1.53	−0.73	0.89
$YbCl_3\mathbf{L}$	mono	1.45	−0.97	1.51	−0.64	0.83
$La(NO_3)_3\mathbf{L}$	bi	2.08	−0.91	1.52	−0.74	0.88
$La(NO_3)_3\mathbf{L}$	mono	2.10	−0.96	1.52	−0.64	0.84
$Eu(NO_3)_3\mathbf{L}$	bi	2.02	−0.91	1.52	−0.74	0.88
$Eu(NO_3)_3\mathbf{L}$	mono	2.04	−0.97	1.53	−0.63	0.84
$Yb(NO_3)_3\mathbf{L}$	bi	1.98	−0.92	1.53	−0.75	0.88
$Yb(NO_3)_3\mathbf{L}$	Mono	1.99	−0.96	1.54	−0.63	0.85

δ^- δ^+ polarization of the O−C and O−P bonds. Hence, the negative charge on the O_P oxygen atom increases by about 0.2 e^- upon complexation, while that on the O_C oxygen atom increases by only 0.1 e^-. In the monodentate binding mode the negative charge on the O_P oxygen atom is further increased (by about 0.05 e^-), while the charge on the O_C oxygen reverts to its value in the free ligand. Interestingly the size of the metal cation has again negligible influence on the electronic structure of the ligand.

The M−**L** binding energies ΔE (Table 1) show that the bidentate binding mode of **L** is preferred in the gas phase. However, the difference $\Delta E_{m/b}$ to the monodentate mode is surprisingly small, ranging from 7.3 kcal mol^{-1} in $LaCl_3$**L** to 4.8 kcal mol^{-1} in $YbCl_3$**L**. It is interesting that the difference is even smaller for the smaller cations. This is a result of repulsive interactions within the first coordination sphere of M^{3+} which impair the bonding of the second oxygen atom and naturally increase with decreasing space around the cation. The explanation for the small $\Delta E_{m/b}$ in general has to be found elsewhere, however. The bond lengths and charges show that the amide fragment is bonded much more weakly to the metal cation than its phosphoryl counterpart. Additionally, the bidentate binding mode enforces a cis conformation on the ligand, which leads to some repulsion between the carbonyl and phosphoryl dipoles and further diminishes the gain from the relatively weak second M−O bond, thus explaining the close values found for the ΔE's of the two conformations. The fact that this is enhanced by the aforementioned steric repulsion in the first shell has an interesting side effect. Generally ΔE increases with decreasing metal ion size. This effect is very small, the difference between La^{3+} and Yb^{3+} being only 3.2 kcal mol^{-1} in the bidentate complexes. However, the same difference is 5.7 kcal mol^{-1} in the monodentate complexes, due to the lowered influence of first shell steric repulsion. This means that the monodentate binding mode leads to a decrease in interaction energies but also to a slight increase in metal cation selectivity.

3.2. $M(NO_3)_3$L Complexes: Role of the Counterions. In this section we will discuss the $M(NO_3)_3$**L** complexes. As they are in many ways similar to the MCl_3**L** complexes, we will only point out the differences between the two types. The NO_3^- anion remained bidentate in the geometry of the complexes, leading to coordination numbers from 7 to 8, depending again on the binding mode of **L**, which is closer to the experimental coordination numbers of the lanthanide cations. One can expect that the increased number of atoms in the first coordination sphere has some influence on the properties of the complexes.

Information on the geometries and binding energies ΔE of the $M(NO_3)_3$**L** complexes can be found in Table 1. The structure of $Eu(NO_3)_3$**L** with both monodentate and bidentate binding of **L** is also depicted in Figure 5. The bidentate complex looks very similar to its $EuCl_3$**L** counterpart. For the monodentate structure one notes that compared to the $EuCl_3$**L** analogue the carbonyl bond is no longer perpendicular to the phosphoryl one and the C−N−C−O moiety is turned slightly toward the metal. This effect is also visible in the PC−CO dihedrals and the nonbonded distance between the amide O_C and the cation, which both become smaller in the monodentate nitrate complexes compared to the chloride complexes. The M−O_P bond length increases in both the monodentate and the bidentate nitrate complexes. This can be explained by the increased steric repulsions between the atoms in the first cation coordination sphere.

Unlike the M−O_P distance, the M−O_C distance decreases from the chloride to the nitrate complexes. This is a result of a force opposing the larger steric effects of nitrate: the nitrate anion is less polarizable than the chloride anion. This leads to a decreased charge transfer from the counterions to the metal cation and in turn to a higher charge on M^{III}, as can be seen from the Mulliken charges in Table 2. This increased cation charge causes a stronger M···**L** Coulomb attraction and in turn both the turning of the C−N−C−O moiety to the metal in the monodentate nitrate complexes and the decreased M−O_C bond length in the bidentate nitrate complexes. The O_P oxygen atom on the other hand experiences a stronger influence from the first shell steric repulsion than from the metal cation charge and therefore increases its distance to M.

A further shortening of the M−O_C bond by 0.03 Å occurs when substituting the methyl groups on P by phenyls (compare $Eu(NO_3)$**L** with $Eu(NO_3)$**L′**, Table 1). When a second ligand **L** is added leading to the complex $Eu(NO_3)_3L_2$, in which both ligands **L** are bound bidentately (Table 1, Figure 5), all M−O distances are larger than in $Eu(NO_3)_3$**L**, due to the further increased steric strain, but the elongation is more pronounced for the O_P oxygen.

The ligand binding energies ΔE of the nitrate complexes (Table 1) are generally around 10 kcal mol^{-1} lower than those of the chloride complexes, due to the increased steric crowding around the cation with the bidentate counterions. The difference between the two complex types increases from La^{3+} to Yb^{3+}, because the repulsions increase with decreasing metal cation size. On the other hand, the difference between chloride and nitrate complexes is always larger with monodentate than with bidentate binding. This is caused by the mentioned increased charge on the metal cation, which is of greater benefit for the bidentate complexes and opposes the lowering of their ΔE's. It should further be noted that the addition of a second bidentate ligand **L** yields less than half of the interaction energy obtained by the addition of the first one and that exchanging the alkyl/aryl substituents on P has nearly no effect on ΔE.

3.3. $Eu(NO_3)_3$LH Complexes: Protonation of CMPO. In this section we will discuss the impact protonation of the ligand **L** has on **L** and the complex $Eu(NO_3)_3$**L**. The questions to be discussed are whether protonation is preferred at the O_P or at the O_C oxygen, whether this is different for the free and complexed ligands, and how it influences the ligand binding energies.

Structural data and, in the case of the complexes, interaction energies ΔE of the protonated species can be found in Table 1, a depiction of the $[\mathbf{L}H]^+$ free ligand in Figure 4, and a depiction of the protonated complex $Eu(NO_3)_3\mathbf{L}H^+$ in Figure 5. As one can see in Figure 4, protonation of the free ligand **L** at either the O_P or the O_C oxygen lets **L** adopt its cis form, due to the formation of a hydrogen bond between the added proton and the unprotonated oxygen atom. Protonation of $Eu(NO_3)_3$**L** leads to very different results, depending on whether it happens at the O_P or the O_C oxygen. In the former case the ligand retains its bidentate binding mode, even though the Eu−O_P bond lengthens by 0.38 Å while the Eu−O_C bond shortens by 0.04 Å and therefore becomes the shorter one of the two. Protonation at the amide

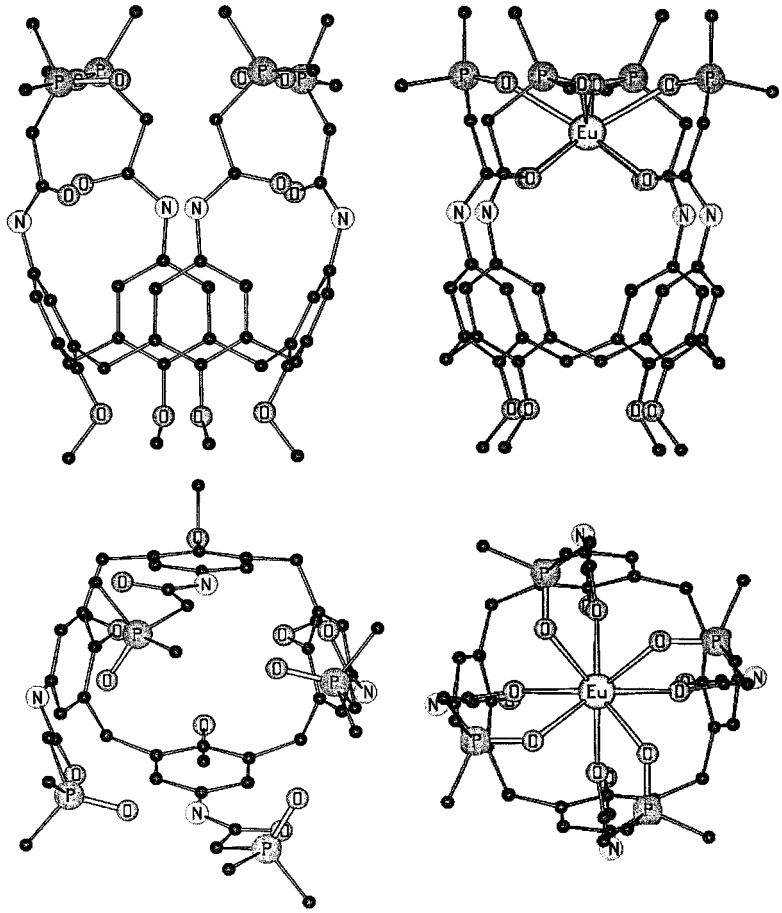

Figure 6. Optimized structures of **Calix** (left) and [Eu**Calix**]$^{3+}$ (right).

O_C on the other hand leads to a complex bound monodentately via the O_P oxygen, with the M−O_P bond shortened by 0.04 Å, still 0.05 Å more than in the unprotonated monodentate complex. In both cases attractive forces between the added proton and neighboring nitrate oxygen atoms are clearly visible.

Which protonation site is preferred in the free ligand **L** is shown by the corresponding reaction energies ΔE. As expected, attaching the proton to the O_P oxygen is more exothermic than attaching it to O_C, the difference being 6.4 kcal mol^{-1}. This changes when the complexed ligand **L** has to be protonated in $Eu(NO_3)_3$**L**. Due to the fact that protonating O_P weakens the strong Eu−O_P bond while protonating O_C leads only to the loss of the less important Eu−O_C interaction, O_C is preferred as protonation site in the complex by 5.6 kcal mol^{-1}. This also means that when the ligand is protonated prior to forming a complex with the metal cation, a proton-transfer reaction is necessary to reach the optimal configuration. However, the interaction energy of [**L**H]$^+$ with $Eu(NO_3)_3$ is only about one-third of the $Eu(NO_3)_3$···**L** interaction energy, making [**L**H]$^+$ an improbable ligand, even under acidic conditions. It should also be noted that while we only discussed the protonation of **L**, protonation of a coordinated nitrate ligand is calculated to be 8.9 kcal mol^{-1} more exothermic.

3.4. [MCalix]$^{3+}$ Complexes: Effect of Grafting CMPO on a Molecular Platform. In this section we discuss the binding of CMPO when attached to a calixarene platform in the **Calix** ligand (see Figure 3), focusing on structural changes from the free to the complexed ligand, on the CMPO binding mode, and the influence of *exo* counterions on the complex.

The free **Calix** ligand and its Eu^{3+} complex are shown in Figure 6; structural data on these compounds, the Yb^{3+} complex, and [$EuCl_2$(**Calix**)]$^+$ can be found in Table 1. We have only calculated one conformer of the free **Calix**, derived from the conformation adopted in an inclusive complex. This free **Calix** has C_2 symmetry. This means that neighboring arms are not equivalent. However, upon complexation this changes, and both the Eu^{3+} and Yb^{3+} inclusive complexes are of C_4 symmetry. As a test on the perturbation brought about by external counterions, we decided to place two chloride anions outside the **Calix** cage of [Eu(**Calix**)]$^{3+}$, near the metal cation. Optimization of this complex leads to a change to C_2 symmetry for the calixarene arms, while the platform itself remains C_{4v}.

If one compares the binding of **Calix** with the bidentate binding mode of **L**, one interesting difference is the larger PC−CO dihedral, which leads to helicity in the M**Calix**$^{3+}$ complexes. The increase is caused by the staggered conformation the O_P and O_C atoms attain, to minimize O···O repulsions. Another important difference concerns the relation between the M−O_P and M−O_C bond lengths. Compared to the EuX_3**L** complexes the M−O_P bonds get much longer (by 0.11 Å with Eu^{3+} and by 0.12 Å with Yb^{3+}) in the **Calix** complexes, while the M−O_C bonds get shorter (by 0.04 with

Table 3. HF and Experimental Results for Selected Compounds with Distances A−B in Å, Dihedrals A−B−C−D in deg, and HF-Calculated Metal−Ligand Binding Energy ΔE in kcal mol^{-1}

		M−O(P)[a]	M−O(C)[a]	O−P	O−C	M−(NO$_2$)$_I$[a]		M−O(NO$_2$)$_{II}$[a]		M−O(H$_2$)	O−P−C−C	P−C− C−O	ΔE[b]
$UO_2(NO_3)_2$**L**	HF	2.498	2.639	1.493	1.225	2.543	2.542	2.509	2.530		−50.5	−0.3	−45. 3
$UO_2(NO_3)_2$**CMPO**[c]	exp[c]	2.377	2.405	1.512	1.264	2.514	2.522	2.514	2.505		57.8	−54.2	
$[Eu(NO_3)_2(H_2O)$**L**$_2]^+$	HF	2.404	2.505	1.503	1.234	2.545	2.508	2.508	2.533	2.555	−51.2	0.3	
		2.462	2.456	1.504	1.233						56.4	−13.5	
$[Eu(NO_3)_2(H_2O)$**CMPO**$_2]^+$[d]	exp[d]	2.343	2.420	1.504	1.25	2.51	2.56	2.46	2.51	2.43			
		2.344	2.434	1.509	1.26								

[a] M = Eu, U, respectively. [b] See Scheme 1 for definition. [c] Experimental results, see code DIJGAE in Table 4. [c] Experimental results, see ref 52.

Eu^{3+} and by 0.01 Å with Yb^{3+}). This means that while the M−O_P are still shorter than the M−O_C bonds in the **Calix** complexes, the difference is much smaller than in the **L** complexes, indicating that they cannot sufficiently relax around the cation. Furthermore, as bond lengthening most often means bond weakening, the overall cation−**Calix** binding strength is probably lower than one would expect from the **L** complexes, as the more important M−O_P bond is weakened with **Calix** as ligand. This assumption is supported by the fact that both the M−O−P and M−O−C angles are larger in the **Calix** than in the **L** complexes (e.g. M−O−P = 136° and M−O−C = 144° in [Eu**Calix**]$^{3+}$ and M−O−P = 131° and M−O−C = 128° in Eu(NO$_3$)**L**), which suggests that the oxygen binding sites in **Calix** do not achieve optimal binding. Another difference between **Calix** and **L** complexes is that the counterions are not directly coordinated to the metal in the former. For comparison we have also calculated the complex [Eu**L**$_4$]$^{3+}$, which can be understood as [Eu(**Calix**)]$^{3+}$ without the calixarene platform. It turns out that the M−O(P) bonds in [Eu**L**$_4$]$^{3+}$ are somewhat shorter than in [Eu(**Calix**)]$^{3+}$ (by 0.016 Å), but the M−O(C) bonds remain about the same, and therefore the difference between the phosphorous and amide oxygen binding is almost as small as in the Calix complex. The helicity of [Eu**L**$_4$]$^{3+}$ and the M−O−P and M−O−C angles are also comparable to [Eu(**Calix**)]$^{3+}$, which means that the major changes in the binding of **L** are not a consequence of the calixarene platform. This is also evident in the energy difference between [Eu**L**$_4$]$^{3+}$ in the [Eu(**Calix**)]$^{3+}$ structure and its fully relaxed geometry: It is only 3.0 kcal/mol.

One could expect that conformational properties of the **Calix** ligand change with different metal cation sizes, but this is not the case. Overall the structure of **Calix** remains about the same with Eu^{3+} or Yb^{3+} as metal cation. This does not suggest a high selectivity of the **Calix** ligand forming inclusive 1:1 complexes.

3.5. Complex [$UO_2(NO_3)_2$L]: A CMPO−Actinide Complex. In many respects actinide cations are very different from their lanthanide analogues, so not all conclusions are transferable between the two. As actinides, due to their active f orbitals,[80] are computationally more demanding than lanthanides, an exhaustive comparison between lanthanide−CMPO and actinide−CMPO binding is beyond the scope of this work. Instead we chose to use one example of an uranyl−CMPO complex, namely [$UO_2(NO_3)_2$**L**], to evaluate some important distinctions.

(80) Schreckenbach, G. *Inorg. Chem.* **2000**, *39*, 1265−1274.

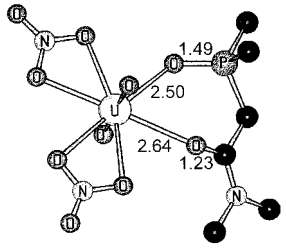

Figure 7. Structure of the calculated $UO_2(NO_3)_2$**L** complex.

The complex [$UO_2(NO_3)_2$**L**] is shown in Figure 7; structural data can be found in Table 3. The oxygen binding sites of **L** and of the nitrate anions are all in the equatorial plane of uranyl, giving the first shell around the uranium atom the shape of a distorted hexagonal bipyramid. The M−O bond distances are comparable to those in the La^{3+} complexes, with the U−O_P bond being somewhat longer than the La−O_P bonds and the U−O_C and La−O_C bonds having nearly the same length. This means that the difference in phosphoryl vs amide binding contributions is smaller in the uranyl than in the lanthanum complexes. The bond length difference is still about 0.14 Å, though, again making O_P the more important binding site compared to O_C. In line with our results for the lanthanide complexes the lengthening of the U−O_P bond compared to the La−O_P bond corresponds to a weaker overall M−**L** interaction energy ΔE, and in fact the uranyl−**L** complex is the weakest of the complexes with a single bidentate ligand **L**. This follows the cation charges, lower for UO_2^{2+} than for La^{3+}, and the experimental result according to which M^{3+} ions are extracted by CMPO in conditions where uranyl is not.[81] The ligand **L** itself has nearly the same conformation as in the bidentate lanthanide complexes.

3.6. Comparisons between Gas-Phase-Calculated and Solid-State Structures. This section is intended to provide some comparisons between the QM-optimized structures and those obtained in the solid state from X-ray diffraction experiments. Strictly speaking, they may differ, as the geometry adopted in a crystal is not only the result of its intrinsic (gas phase) properties but also of the external influence of packing effects and the crystal field created by

(81) Preliminary results on Cm(NO$_3$)$_3$**L** show that the Cm−O_P and Cm−O_C bonds are 0.07 Å and 0.08 Å longer, respectively, than the corresponding bonds in the analogue Eu^{3+} complex. These differences are somewhat larger than the difference in ionic radii (0.95 Å for Eu^{3+} and 0.97 Å for Cm^{3+}). The M−**L** binding energy in Cm(NO$_3$)$_3$**L** is −51.1 kcal mol^{-1}, compared to −52.3 kcal mol^{-1} in Eu(NO$_3$)$_3$**L**. This shows that Ac^{3+}−**L** bonds are similar to Ln^{3+}−**L** bonds. Cm^{3+}'s higher cation charge and strong preference for the O_P binding site let it form stronger complexes than uranyl (−45.3 kcal mol^{-1}).

Table 4. Lanthanide and Uranyl Complexes of CMPO Type Ligands from the Cambridge Structural Database (CSD)

ref code[f]	compd	coord[a]	CN_M[b]
DODVAT[1]	$Nd(NO_3)_3$**CMPO**$_2$	bi	10
BIZFIZ[2]	$Sm(NO_3)_3$**CMPO**$_2$	bi	10
GIBTAM[3]	$Gd(NO_3)_3(H_2O)$**CMPO**$_2$	mono	9
WAGJOD[4]	$Gd(NO_3)_3$**CMPO**	bi[c]	9
CIKTOF[5]	Dy(NS)**CMPO**$_2$	bi[c]	7
BIZFOF[2]	$Er(NO_3)_3(H_2O)$**CMPO**$_2$	mono	9
DOGKEP[6]	$Er(NO_3)_3(H_2O)$**CMPO**$_2$	mono	9
GEGXOF[7]	$Er(NO_3)_3$**CMPO**	bi[d]	9
WAGFOZ[8]	$Er(NO_3)_3$**CMPO**	bi[c]	9
WAGFUF[8]	$Er(NO_3)_3$**CMPO**$_2$	bi/mono	9
BOXPIN[9][e]	$UO_2(NO_3)_2$**CMPO**	bi	8

[a] Bidentate (bi) or monodentate (mono) binding. [b] Coordination number of the lanthanide M^{3+}. [c] Bridging ligand (via oxygen in side chain). [d] Tridental ligand (additional amide group). [e] General compound formula, coordination mode, and coordination number are the same for the other uranyl−CMPO compounds in the CSD: DIJFUX;[10] DIJGAE;[10] HOTSAK;[11] SUDPUC;[12] VOMHAG;[13] WAGFIT.[8] [f] (1) Caudle, L. J.; Duesler, E. N.; Paine, R. T. *Inorg. Chem.* **1985**, *24*, 4441. (2) Bowen, S. M.; Duesler, E. N.; Paine, R. T. *Inorg. Chim. Acta* **1982**, *61*, 155. (3) McCabe, D. J.; Duesler, E. N.; Paine; R. T. *Inorg. Chim. Acta* **1988**, *147*, 265. (4) Conary, G. S.; McCabe, D. J.; Meline, R. L.; Duesler, E. N.; Paine, R. T. *Inorg. Chim. Acta* **1993,** *203*, 11. (5) Bowen, S. M.; Duesler, E. N.; Paine, R. T. *Inorg. Chim. Acta* **1984**, *84*, 221. (6) McCabe, D. J.; Duesler, E. N.; Paine, R. T. *Inorg. Chem.* **1985**, *24*, 4626. (7) McCabe, D. J.; Duesler, E. N.; Paine, R. T. *Inorg. Chem.* **1988**, *27*, 1220. (8) Conary, G. S.; Meline, R. L.; Schaeffer, R.; Duesler, E. N.; Paine, R. T. *Inorg. Chim. Acta* **1992**, *201*, 165. (9) Bowen, S. M.; Duesler, E. N.; Paine, R. T. *Inorg. Chem.* **1983**, *22*, 286. (10) Caudle, L. J.; Duesler, E. N.; Paine, R. T. *Inorg. Chim. Acta* **1985**, *110*, 91. (11) Cherfa, S.; Pecaut, J.; Nierlich, M. *Z. Kristallogr.* **1999**, *214*, 523. (12) Karthikeyan, S.; Paine, R. T.; Ryan, R. R. *Inorg. Chim. Acta* **1988**, *144*, 135. (13) Conary, G. S.; Meline, R. L.; Caudle, L. J.; Duesler, E. N.; Paine R. T. *Inorg. Chim. Acta* **1991**, *189*, 59.

its neighbors. In a previous study we have shown that consideration of such a field, for example by self-consistent reaction field methods, can change lanthanide−ligand bond lengths by around 0.05 Å.[41] Furthermore, investigations in the Cambridge Structural Database (CSD)[82] show that the M−O bonds between a given lanthanide or actinide cation and CMPO ligands show much variation in their lengths. For example, experimental results for $U-O_P$ bonds in CMPO complexes vary by about 0.1 Å (compare for instance the structures with reference codes BOXPIN and HOTSAK from the CSD; see Table 4). This means that the potential energy profile for bond length changes in these complexes is probably quite flat. Also note that the calculated ligand **L** has different substituents compared to the CMPO ligands in the experimental structures, which, according to our test calculation (see methyl vs phenyl substitution above), can cause another 0.03 Å difference.

In the solid state, the CMPO ligand is typically bound bidentately in the lanthanide and actinide complexes, but examples for monodentate binding via O_P do exist. Of the 10 lanthanide−CMPO complexes found in the CSD (see Table 4), seven are bidentate and three monodentate, while all of the seven uranyl CMPO complexes retrieved are bidentate. In the monodentate lanthanide complexes O_C is stabilized by a hydrogen bond to a water molecule coordinated to the same lanthanide cation. We could not find any case of monodentate binding via O_C. The dominance of the bidentate mode is in agreement with our calculated binding energies, which show that the bidentate binding mode is intrinsically preferred but that the energy difference between monodentate and bidentate binding is not large. In the bidentate complexes the $M-O_P$ bond is generally shorter than the $M-O_C$ bond, in agreement with our calculated structures. Counterexamples exist, however (e.g. the structure with reference code WAGFUF; see Table 4).

We will now compare the calculated distances in one lanthanide and one actinide complex with their experimental analogues (see Table 3), selecting for this purpose $[\mathbf{L}_2Eu(NO_3)_2(H_2O)]^+$ and $\mathbf{L}UO_2(NO_3)_2$, respectively. Note that the ligands of the experimental compounds differ from the calculated ones by the substituents used. In the case of the $[\mathbf{L}_2Eu(NO_3)_2(H_2O)]^+$ complex a notable difference between calculation and experiment is that the two ligands **L** are bound to Eu^{3+} with very similar distances in the X-ray structure but with quite different distances in the calculated structure. However, such behavior is known from other experimental structures as well.[83] For our comparison we will thus use the average values. The average $Eu-O_P$ distances in the calculated and experimental structure differ by 0.09 Å, and the difference between the $Eu-O_C$ distances is 0.05 Å. The calculated bonds are almost always longer than the experimental ones. This difference gets larger for the water ligand, where it rises to 0.12 Å. Interestingly, the agreement is better for the charged nitrate ligands, which on average are calculated to be 0.01 Å longer than in the X-ray structure. The agreement for the internal bonds of **L** is comparable to this value.

In the case of the $\mathbf{L}UO_2(NO_3)_2$ complex the $U-O_P$ bond is 0.12 Å longer in the calculation, while the $U-O_C$ bond is 0.23 Å longer. Again the agreement for nitrate ligands is much better; here the difference is only 0.02 Å. The Eu−**L** bonds still show a satisfactory agreement, while the calculated U−**L** distances are considerably longer than the experimental ones.

3.7. Methodological Issues: Influence of Electron Correlation. While electron correlation can certainly be expected to influence many of the properties of the compounds studied in this work, we are mostly concerned with the differences between the various complexes, for which correlation effects should be small.[84,85] However, to verify this we have conducted some test calculations on **L** and selected MCl_3**L** complexes on the DFT level. The results are summarized in Table 5. Compared to the HF level, the O−P and O−C bond lengths within the ligand **L** increase, by about 0.01 Å in the case of the O−P and by about 0.02 Å in the case of the O−C bond. The M−O bonds behave differently. $M-O_P$ lengthens by about 0.01 Å in the bidentate binding mode and remains the same in the monodentate one, while $M-O_C$ shortens, albeit by less than 0.005 Å. Even though this means that in some cases the difference between the $M-O_P$ and $M-O_C$ bond lengths decreases due to the

(82) Allen, F. H.; Kennard, O. *Chem. Des. Autom. News* **1993**, *8*, 31−37.

(83) Cherfa, S. Thesis, Université de Paris-Sud, 1998.

(84) Cosentino, U.; Moro, G.; Pitea, D.; Calabi, L.; Maiocchi, A. *J. Mol. Struct. (THEOCHEM)* **1997**, *392*, 75−85. Joubert, L.; Picard, G.; Legendre, J.-J. *Inorg. Chem.* **1998**, *37*, 1984−1991.

(85) Glendening, E. D.; Petillo, P. A. *J. Phys. Chem. B* **2001**, *105*, 1489−1493.

Table 5. DFT (B3LYP) Results for Selected Compounds with Distances A−B in Å, Dihedrals A−B−C-D in deg, and Metal−Ligand Binding Energies ΔE in kcal mol^{-1}

	coord[a]	M−O(P)[b]	M−O(C)[b]	O−P	O−C	M−O(NO$_3$)$_I$[b]		M−O(NO$_3$)$_{II}$[b]		M−O(NO$_3$)$_{III}$[b]		O−P−C− C	P−C−C−O	ΔE[c]
L	trans			1.488	1.223							−70.7	−90.4	
La(NO$_3$)$_3$**L**	bi	2.478	2.640	1.510	1.244	2.592	2.598	2.516	2.564	2.533	2.524	−58.2	3.2	−45.3
Eu(NO$_3$)$_3$L	bi	2.378	2.526	1.509	1.245	2.519	2.459	2.44 8	2.431	2.431	2.422	−56.9	4.1	−45.5
Eu(NO$_3$)$_3$**L**	mono	2.277	4.743	1.522	1.226	2.493	2.428	2.405	2.438	2.395	2.443	−61.1	−20.3	−39.2

[a] Bidentate (bi) or monodentate (mono) binding. [b] M = La and Eu, respectively. [c] See Scheme 1 for definition.

influence of electron correlation effects, the impact is not large enough to change any of our conclusions. Interaction energies ΔE consistently decrease on the DFT level, without changing their order, as found in related complexes.[38,41] The difference between La^{3+} and Eu^{3+}, which is already small on the HF level, almost vanishes on the DFT level, though, while the $\Delta E_{m/b}$ difference between monodentate and bidentate binding nearly stays the same.

4. Discussion and Conclusion

We have presented a quantum mechanical study of lanthanide complexes with the CMPO type ligand **L** and the ligand **Calix**, where four **L** are attached to a calixarene platform. Our gas-phase Hartree−Fock calculations with relativistic ECP's yield structures in very good agreement with X-ray measurements for the lanthanide and uranyl bonds with anionic ligands and satisfactory agreement for the bonds between lanthanides and neutral ligands. Uranyl bonds with neutral ligands are represented with qualitative accuracy. The inclusion of electron correlation on the DFT level, using the hybrid functional B3LYP, does not significantly change the results. In the following, we summarize the most important results concerning the binding mode of **L**, the influence of counterion related steric crowding on cation selectivity, and the effects of grafting **L** onto a molecular platform.

4.1. Bidentate Effect and Importance of Steric Crowding. Our calculations show that **L** always prefers the bidentate binding mode in the gas phase but that the difference to monodentate binding via the phosphorus oxygen atom is surprisingly small. The low preference of **L** for bidentate binding, despite the energy gain from an additional M−O interaction, can be attributed to the *importance of steric interactions* (repulsions) within the first coordination sphere of the metal. The intraligand part of these interactions stems from the repulsion between two intrinsic dipoles of **L**, $O^{\delta-}$−$P^{\delta+}$ and $O^{\delta-}$−$C^{\delta+}$, that are forced into a parallel arrangement upon bidentate binding. Their mutual repulsion is enhanced by the polarizing effect of the cation charge, which adds an induced dipole moment to their permanent dipole moments. The interligand part of the steric interactions is the repulsion between the counterions and the oxygen binding sites of **L** within the first coordination sphere of the cation. It is partly Coulombic repulsion between negative (partial) charges and partly avoided overlap of electron clouds ("steric crowding"). This effect is augmented in the bidentate complexes due to the added oxygen atom bound to the cation.

The mentioned intraligand interaction can be demonstrated by an isodesmic reaction, in which a ligand **L** bound bidentately to $EuCl_3$ is exchanged with two monodentate,

Scheme 2. Isodesmic Reaction Exchanging One Bidentate Ligand with Two Monodentate Ones Coordinated to $EuCl_3$

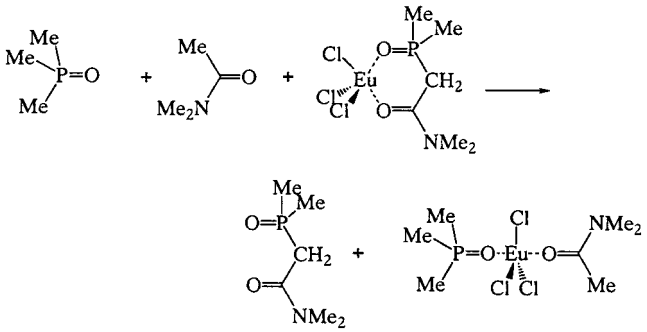

monofunctional ligands bearing analogous substituents, i.e. $Me_2NC(O)Me$ and $Me_3P(O)$, respectively (Scheme 2). According to our calculations, the reaction is exothermic by 27.1 kcal mol^{-1}, which means that the two monodentate ligands are markedly preferred over one bidentate ligand **L**. The main reason for this finding is that the O−C and O−P dipoles can avoid each other (they assume trans positions) and therefore the intraligand repulsion caused by the parallel dipoles within the bidentately bound ligand **L** is removed.

As pointed out previously,[40,41] anions are an important contributor to interligand repulsions within the first coordination shell of the cation ("steric crowding"). Their binding sites are more negatively charged than those of neutral coordinated ligands, leading therefore to enhanced electrostatic repulsions with the other ligands in the first coordination sphere, and they are also generally bigger than neutral ligands, also leading to enhanced steric effects (as taken into account, e.g. by van der Waals models in force field approaches[86]). Thus, steric crowding is often intensified with negatively charged ligands (e.g. phosphates and analogues). One can assume that more bulky anions (e.g. bidentate ones such as carboxylates or ligands obtained by O → S substitution) increase the strain around the metal and, therefore, reduce the intrinsic preference for bidentate binding. Conversely, when there are no neutralizing counterions in the first coordination sphere of the metal, bidentate coordination is favored. One extreme case concerns the M**L**$^{3+}$ complexes or protonated **L**H$^+$ species, in which only bidentate structures correspond to an energy minimum.

The metal cation "size" (and hardness) influences both inter- and intraligand interactions. As the ionic radii of the M^{3+} ions decrease from La^{3+} to Yb^{3+} along the lanthanide series, shorter M−**L** and M−counterion bonds lead to more "steric crowding" and interligand repulsions. Additionally the cation gets harder, thereby increasing the polarization

(86) Comba, P. *Coord. Chem. Rev.* **1999**, *182*, 343−371.

of **L** and thus its intraligand dipole−dipole repulsion. Both effects mean that the preference for the bidentate binding mode decreases along the lanthanide series and on going from divalent to trivalent cations. Another parameter of interest concerns substituent effects on the ligands. The calculations have been conducted with methyl groups, but the energy perturbation brought about by other substituents (e.g. aryl groups[19]) may not be negligible, compared to the energy difference between the two binding modes.

What happens in condensed phases is even more complicated, as the first coordination shell is filled by additional ligands, anions, or polar solvent molecules. Furthermore, the small penalty for monodentate binding may be easily compensated for by second shell environment effects, like hydrogen bonding interactions with the uncoordinated carbonyl group (e.g. with coextracted nitric acid or water), which also should make monodentate complexes better solvated in polar solvents and more hydrophilic. All these arguments point to a further reduction of the preference for bidentate binding. It should be noticed, however, that they correspond to enthalpy effects and that entropy effects yield opposite trends. Binding water molecules or additional ligands to monodentate complexes to compensate for a binding site of the ligand imposes some entropy penalty related to its reduced freedom. In the case of cyclic polyamines, compared to single monodentate amines, the importance of entropy effects on the chelate effect has been pointed out.[87] The surprisingly small enthalpy preference calculated here and the experimental result according to which multidentate ligands are generally preferred over groups of unidentate ligands also indirectly point to the importance of entropy on bidentate binding. This is unfortunately hard to monitor experimentally and to predict by current modeling approaches.

4.2. Steric Crowding, Counterions, and Binding Selectivity. L shows little selectivity regarding different metal cations, and its selectivity is strongly influenced by steric effects from crowding the first coordination sphere of the metal cation, resulting from counterions or additional ligands. This is apparent in the changes of the metal selectivity order with different complex types. In the MCl_3**L** complexes the interaction energies ΔE increase with decreasing metal cation size, i.e., $La^{3+} < Eu^{3+} < Yb^{3+}$. If the more spatial demanding nitrate counterion is used in the $M(NO_3)_3$**L** complexes, the order changes to $La^{3+} < Yb^{3+} < Eu^{3+}$. Finally, if some steric strain in these complexes is relieved by changing to the monodentate binding mode of **L**, selectivity changes back to the original order. Thus, *steric crowding may be an important source of binding selectivity*, not only in the lanthanide series but also likely for lanthanide/actinide discrimination.[88]

4.3. Effect of Grafting CMPO on a Molecular Platform. If CMPO is attached to a calixarene as a lipophilic platform, forming the ligand **Calix**, inclusive complexes show a strong change in the conformation of the CMPO moiety, compared to the free ligand, which hints at relatively unfavorable binding conditions. Formation of such inclusive complexes may also not be desirable for extraction purposes, as the hydrophilic counterions extracted to achieve the electroneutrality of the system are poorly solvated. A better situation occurs when M^{3+} and X^- species form intimate ion pairs, as in most solid-state structures. This precludes, however, the formation of inclusive complexes such as M**Calix**$^{3+}$. The latter are calculated to be of C_4 symmetry. The 4-fold arrangement, although consistent with earlier molecular dynamics results,[53] is somewhat surprising, as NMR studies of calixarene lanthanide complexes suggest C_2 symmetry for the complexed ligand as well.[89] There are several possible explanations for this discrepancy. One is that, in solution, calixarene ligands form complexes similar to those found in the solid state, where the calixarene ligand arms are bound to different metal cations,[82] and therefore, noninclusive complexes with lower symmetries are formed. Another possible explanation for the lower symmetry found in the NMR experiments is the influence of counterions, but anions surrounding the complex are barely sufficient to lower the symmetry of the cone. This suggests that, in solution, the complexes may not be inclusive and of 1:1 stoichiometry but form aggregates, as indicated by the aforementioned NMR studies on **Calix** complexes and by small-angle neutron diffraction studies on analogous complexes with phosphoryl-containing ligands.[90, 91]

What happens in complex solvent environments cannot presently be assessed by QM calculations alone and requires accounting for the dynamic features of the system. However, the static gas-phase results presented here serve as a valuable reference, not only for M^{3+} complexes of CMPO type ligands but also for other potentially bidentate ligands such as diamides, picolinamides,[23,92] or bis(phosphoryl) compounds.[19,93]

Acknowledgment. The authors are grateful to the CNRS IDRIS and Université Louis Pasteur for computer resources and to the EEC (FIKW-CT-2000-0088 contract) and PRACTIS for support.

IC010658T

(87) Martell, A. E.; Hancock, R. D.; Motekaitis, R. J. *Coord. Chem. Rev.* **1994**, *133*, 39−65 and references therein.

(88) Ionova, G.; Ionov, S.; Rabbe, C.; Hill, C.; Madic, C.; Guillaumont, R.; Modolo, G.; Krupa, J.-C. *New J. Chem.* **2001**, *25*, 491−501.

(89) Lambert, B.; Jacques, V.; Shivanyuk, A.; Matthews, S. E.; Tunayar, A.; Baaden, M.; Wipff, G.; Böhmer, V.; Desreux, J.-F. *Inorg. Chem.* **2000**, *39*, 2033−2041.

(90) Chiariza, R.; Urban, V.; Thiyagarajan, P.; Herlinger, A. W. *Solvent Extr. Ion Exch.* **1999**, *17*, 113−132.

(91) Diamond, H.; Thiyagarajan, P.; Horwitz, E. P. *Solvent Extr. Ion Exch.* **1990**, *8*, 503−513.

(92) Iveson, P. B.; Drew, M. G. V.; Hudson, M. J.; Madic, C. *J. Chem. Soc., Dalton Trans.* **1999**, 3605−3610.

(93) Rozen, A. M. *J. Radioanal. Nucl. Chem.* **1990**, *143*, 337−355.